Available online at www.sciencedirect.com
ScienceDirect
Journal of Solid State Chemistry 179 (2006) 2998–3006
JOURNAL OF SOLID STATE CHEMISTRY
www.elsevier.com/locate/jssc

The reciprocal $CuInS_2 + 2CdSe \Leftrightarrow CuInSe_2 + 2CdS$ system—Part II: Liquid–solid equilibria in the system

O.V. Parasyuk[a,*], I.D. Olekseyuk[a], V.I. Zaremba[b], O.A. Dzham[a], Z.V. Lavrynyuk[a], L.V. Piskach[a], O.G. Yanko[c], S.V. Volkov[c], V.I. Pekhnyo[c]

[a]*Department of General and Inorganic Chemistry, Volyn State University, Voli Ave 13, Lutsk 43009, Ukraine*
[b]*Department of Inorganic Chemistry, Ivan Franko National University of L'viv, 6 Kyryla and Mefodiya St., L'viv 79005, Ukraine*
[c]*V.I. Vernadskii Institute for General and Inorganic Chemistry of the Ukrainian National Academy of Sciences, Palladina Ave 32-34, Kyiv 03680, Ukraine*

Received 12 February 2006; received in revised form 18 May 2006; accepted 20 May 2006
Available online 7 June 2006

Abstract

The phase equlibria in the reciprocal system $CuInSe_2 + 2CdS \Leftrightarrow CuInS_2 + 2CdSe$ were investigated by differential thermal and X-ray phase analysis. The phase diagrams of a series of vertical sections, a liquidus surface projection and a spatial phase diagram were constructed. It was established that the addition of cadmium chalcogenides leads to the stabilization of the cubic modifications of the ternary compounds, which form a continuous solid solution series, at the annealing temperatures. The boundaries of the solid solutions were determined by the change of the unit cell parameters; the isothermal sections at 620 and 870 K were constructed.

Keywords: Semiconductors; Liquid–solid reaction; Phase diagrams; Thermal analysis

1. Introduction

The search for new efficient materials for the photovoltaic conversion of solar energy among the complex chalcogenides remains a hot topic in the last decade [1–3]. These materials are commercially relevant by their price/efficiency ratio [4] and are already used in the industrial production of solar modules. Currently, $CuInSe_2$ (CIS) and $CuIn_{1-x}Ga_xSe_2$ (CIGS) have found practical application [1–3]. The efficiency of the solar radiation conversion by the thin-film elements based on these materials is 18% and 20% [1–6], respectively. Their advantage over the classic materials of the absorption layer of the solar elements (Si, GaAs) are primarily economic aspects [4] and certain specific characteristics, e.g. high radiation resistance (approximately 50 times higher) [7–9]. It is also important that the radiation damage is regenerated by their thermal processing at 470–520 K during 10–15 min [10].

The developments based on other compounds with the chalcopyrite structure are also promising (mostly $CuInS_2$, e.g. [11,12]). The solid solutions based on these materials are investigated as well, in 4-element $CuIn(S,Se)_2$ [13,14] and 5-element $Cu(In,Ga)(S,Se)_2$ [15,16] chalcogenide phases. The major challenges in this research are the search for the optimal composition of the solid solutions and the technological improvement of thin film deposition.

There is currently no material that would fully satisfy the requirements [1,2], therefore the search for the optimal composition is a promising problem that is investigated in the latest years by a wide front of research groups.

The $CuInSe_2$ compound is a semiconductor of either *p*- or *n*-type conductivity (depending on the technological conditions of its production) with a bandgap energy, measured by various authors, in the 0.96–1.1 eV range [17]. The industrial production of solar cells utilizes a heterojunction $CuInSe_2$/CdS. Though the current trend is to substitute CdS with a less toxic material, the most efficient cells were based on it [1–3]. It is known that Cu^+ ions have high diffusion coefficient [18]. Therefore, the information on possible solid-state processes (solid solubility, the

*Corresponding author. Fax: +38 03322 41007.
E-mail address: oleg@lab.univer.lutsk.ua (O.V. Parasyuk).

0022-4596/$ - see front matter © 2006 Elsevier Inc. All rights reserved.
doi:10.1016/j.jssc.2006.05.036

formation of new phases) at the interface is important. This knowledge can be derived from a phase diagram of a system composed of these compounds. The $CuInSe_2$–CdS system should be considered as an integral part of the reciprocal system $CuInSe_2 + 2CdS \Leftrightarrow CuInS_2 + 2CdSe$ that is investigated in this paper. Though the system is composed of four compounds, it is not a quaternary one because a chemical reaction is possible in the system. Such systems, according to Anosov et al. [19], belong to the chemical systems. The number of independent components in such systems equals the number of original system components (4) less the number of chemical reactions that occur in the system (1). Therefore, the number of independent components is 3 and the system is a ternary one.

An interesting benefit is a possible decrease of the cost of solar cells due to the partial substitution of indium with the solid solutions of the reciprocal system.

2. Quasi-binary systems

2.1. The CdS–CdSe system

The CdS–CdSe system is quasi-binary, type I of Roozeboom classification [20], complete miscibility, which agrees well with the fact that the compounds are isostructural. The concentration dependence of the unit cell parameters is linear [20–22].

2.2. The $CuInSe_2$–$CuInS_2$ system

The phase diagram of the $CuInSe_2$–$CuInS_2$ system was studied in [23,24]. The authors [23] established that the system was characterized by continuous solid solution series of α- and γ-solid solutions with tetragonal (low-temperature, LT, modification) and cubic (high-temperature HT(1)) structure and a region of β-solid solutions of high-temperature HT(2) modification of $CuInS_2$ ranging from 0 to 30 mol% $CuInSe_2$. The authors [24] analyzed a possible formation in the system of two compounds that formed a continuous solid solution series between themselves and with the system components. Two phase transitions were recorded, one of which occurred in all the system alloys, whereas another one, HT(2), was typical only of alloys in the range of 67–100 mol% $CuInS_2$.

2.3. The $CuInS_2$–CdS system

In the previous work, the authors investigated the phase diagram of the $CuInS_2$–CdS system [25]. A continuous solid solution series formed in the system between the HT(2) modification of $CuInS_2$ that has a wurtzite structure and CdS which is isostructural to it. Another HT(1) $CuInS_2$ modification that crystallizes in the sphalerite structure was stabilized at the annealing temperature by the addition of cadmium sulfide, and existed in the ~37–44 mol% CdS range at 870 K. The decrease of the range of this solid solution at lower temperature led us to a suggestion about a possibility of a solid-state decomposition below 870 K. To confirm or disprove it, we performed an additional annealing of four alloys at 670 K. X-ray phase analysis showed that all these alloys were two-phase, containing a mixture of either tetragonal and cubic or cubic and hexagonal phases. Thus, we have confirmed the existence of the cubic phase at this temperature as well, though the homogeneity region of β-solid solutions was not determined precisely. The alloys of this region exhibited *p*-type conductivity and large values of thermo-EMF (~1250 μV/K).

2.4. The $CuInSe_2$–CdSe system

The investigation of the phase diagram of this system was reviewed in the first part of this study [26].

3. Experimental

Two series of alloys were prepared for the investigation of the phase equilibria in the $CuInSe_2 + 2CdSe \Leftrightarrow CuInS_2 + 2CdSe$ system, their composition and location are shown in Fig. 1. The alloys were synthesized from high-purity elements (at least 99.99 wt% purity). Calculated amounts of elements were placed into the quartz ampoules which were evacuated and soldered. At the first stage, the

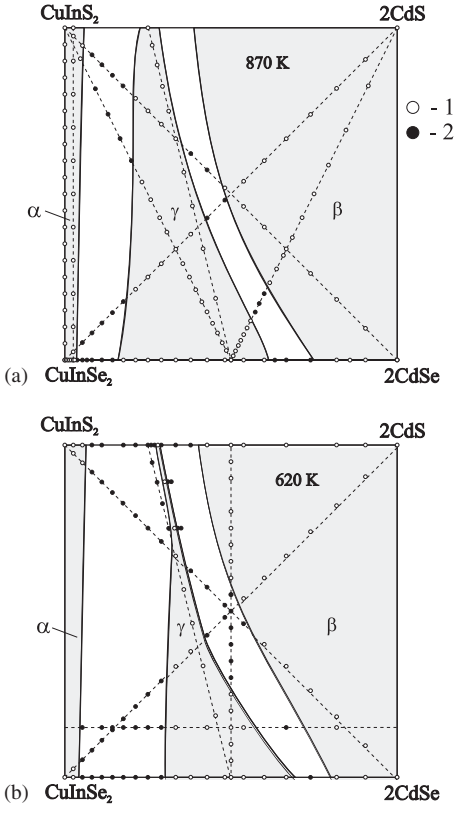

Fig. 1. Chemical and phase composition of the alloys and isothermal sections of the reciprocal system $CuInSe_2 + 2CdS \Leftrightarrow CuInS_2 + 2CdSe$ at 870 K (a) and 620 K (b) (1, single-phase alloys; 2, two-phase alloys).

Table 1
Composition of the primary phase in the alloys of the '$Cu_3Cd_2In_3S_8$'–'$CuCd_2InSe_4$' section (EDX analysis data)

Composition, mol% '$Cu_2CdInSe_4$'	Cu	Cd	In	S	Se
0	15.90	14.84	19.01	50.25	—
10	16.06	15.28	18.32	47.91	2.42
20	20.03	12.02	20.38	43.66	3.91
30	19.29	14.18	19.45	40.80	6.29
40	16.53	16.30	18.78	37.19	11.20

ampoules were heated in the oxygas burner flame to complete reaction of elementary sulfur. Then the containers were placed in the shaft-type furnace and heated at the rate of 40–50 K/h. The maximum synthesis temperature was 1420 K for all alloys. After the exposure to this temperature for 6 h with periodic vibration, the alloys were cooled (10 K/h) to the annealing temperature. The first series of the alloys were annealed for 500 h at 870 K, the second one, at 620 K during 1440 h. The annealing temperatures correspond to the upper and the lower boundaries of the temperature range of the industrial thin film deposition of the chalcopyrites in the production of the photovoltaic elements [1]. The alloys were then quenched into cold water. Obtained alloys were black compact ingots. The alloys near $CuInSe_2$ were typically brittle. Some alloys with high CdS content were inhomogeneous after the reported synthesis process. Those were additionally crushed into powder in an agate mortar, pressed into tablets and reheated according to the second stage of the synthesis. Obtained alloys were investigated by differential thermal (a Paulik–Paulik–Erdey derivatograph) and X-ray phase analysis (a DRON 4-13 diffractometer, CuK_α radiation). The lattice parameters were computed using PDWin-2 program package. The microstructure of polished alloys was observed at a Leica VMHT Auto microhardness tester. For the EDX analysis of the bulk samples, irregularly shaped pieces were embedded in a metacrylate matrix, polished and then examined in the scanning electron microscope (LEICA 420 I) in back-scattering mode. Cu, Cd, InAs, FeS_2, Se were used as standards. No impurity elements heavier than sodium have been observed. The experimentally determined compositions (Table 1) were close to the initial compositions of the samples.

4. Triangulation

According to the X-ray phase analysis data, the isothermal sections of the reciprocal system $CuInSe_2 + 2CdS \Leftrightarrow CuInS_2 + 2CdSe$ contain three single-phase fields of solid solutions (Fig. 1), two of which are stretched along the side systems of the quadrangle which form the continuous solid solution series (α- and β-solid solutions), and the third one is located between them (γ-solid solutions). The plots show that the decrease of temperature leads to narrowing of the homogeneity regions of the solid solutions. This is especially remarkable for γ-solid solutions in sulfur-rich alloys. It makes possible an assumption that at some lower temperature we should expect a decomposition by a eutectoid process of the solid solution in the $CuInS_2$–2CdS system in the sulfur-rich part of the quadrangle that would result in the existence of a three-phase field in that region.

The formation of γ-solid solutions means that none of the sections corresponding to the quadrangle diagonals is quasi-binary, which has its consequences in the change of the lattice parameters in the two-phase regions of the system sections. Therefore, the $CuInSe_2 + 2CdS \Leftrightarrow CuInS_2 + 2CdSe$ system belongs, according to the classification set out in [19], to reversible reciprocal systems.

5. Results

5.1. The $CuInS_2$–$CuInSe_2$ system (Fig. 2)

Our results confirm the formation of two continuous solid solution series in the $CuInS_2$–$CuInSe_2$ system. The solid solution range of the HT(2) $CuInS_2$ modification is limited and decomposes by a metatectic process $\beta \Leftrightarrow \gamma + L$. The invariant point coordinates are 31 mol% $CuInSe_2$ at 1315 K (Fig. 3). The change of the unit cell parameters of the α-phase is linear.

5.2. The $CuInS_2$–CdS system at 620 K (Fig. 3)

As the phase diagram of this system was constructed earlier [24] during the study of the alloys annealed at 870 K, in this paper we only established the boundaries of the solid

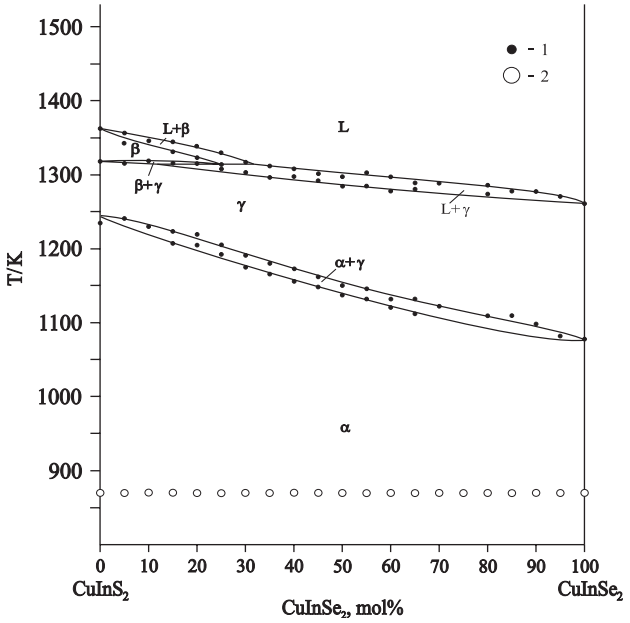

Fig. 2. Phase diagram of the $CuInSe_2$–$CuInS_2$ system (1, DTA results; 2, single-phase alloys).

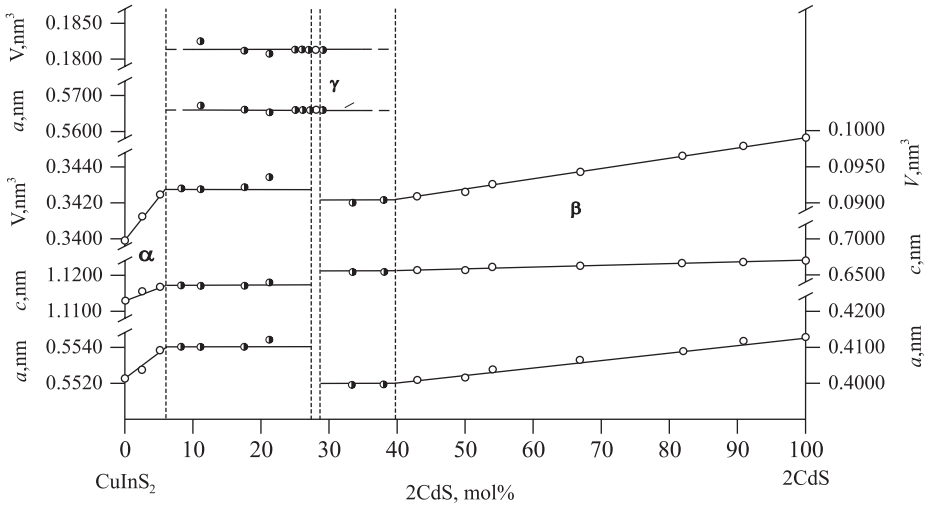

Fig. 3. Plots of the lattice parameters and unit cell volumes of the $CuInS_2$–CdS section alloys at 620 K.

solutions at 620 K. The change of the lattice parameters of the system alloys at this temperature is shown in Fig. 3. The α-solid solution has a homogeneity region in the 0–6 mol% 2CdS range. The γ-phase at the annealing temperature has a minor homogeneity region that is smaller and more shifted to the CdS side than at 870 K. The solid solution range of CdS (β) at the annealing temperature extends from ~40 to 100 mol% 2CdS.

5.3. The '$Cu_{0.974}Cd_{0.052}In_{0.974}S_2$'–'$Cu_{0.974}Cd_{0.052}In_{0.974}Se_2$' section (Fig. 4)

The '$Cu_{0.974}Cd_{0.052}In_{0.974}S_2$'–'$Cu_{0.974}Cd_{0.052}In_{0.974}Se_2$' section (Fig. 4) is parallel to the quadrangle side $CuInS_2$–$CuInSe_2$; it was necessary to establish the position of the monovariant line and to refine the homogeneity region of α-solid solution. The section liquidus is represented by one line of the primary crystallization of β-solid solution. The sub-liquidus part contains a field of secondary crystallization and a field of primary crystallization of γ-phase. Such placement of the phase fields is caused by the incongruent character of the monovariant curve (Figs. 12 and 13). At lower temperatures, the section crosses the field of γ-solid solutions, the region of the coexistence of γ- and α-phases and the field of α-solid solutions. At 870 K, all alloys are of single phase and crystallize in the chalcopyrite structure. The changes of the unit cell parameters are linear.

5.4. The '$CuCd_2InSe_4$'–'$Cu_3Cd_2In_3S_8$' section (Figs. 5 and 6)

The '$CuCd_2InSe_4$'–'$Cu_3Cd_2In_3S_8$' section is of interest because it crosses the homogeneity region of γ-solid solutions which at 870 K occupies the entire concentration range (Fig. 5). Above the annealing temperatures, the section consists of four lines, two of which correspond to the section liquidus and solidus, and two others are related to the transition from cubic⇔tetragonal phase. The

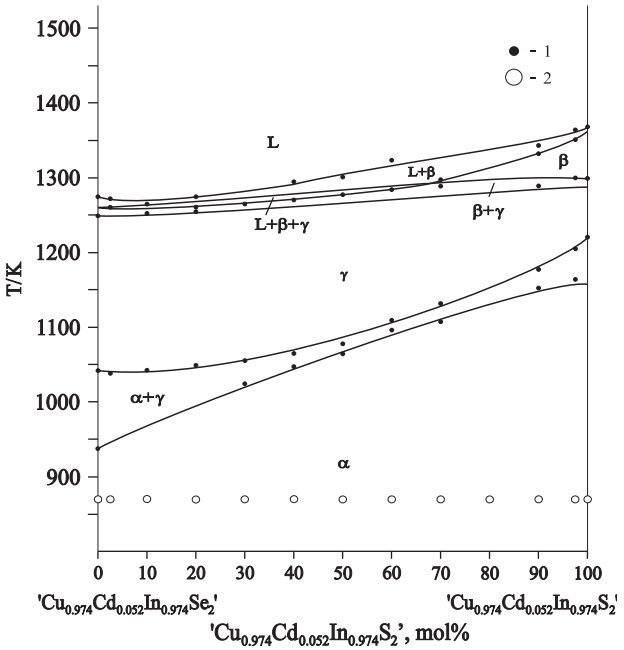

Fig. 4. Phase diagram of the '$Cu_{0.974}Cd_{0.052}In_{0.974}S_2$'–'$Cu_{0.974}Cd_{0.052}In_{0.974}Se_2$' section (1, DTA results; 2, single-phase alloys).

change of the unit cell parameters of the section alloys is shown in Fig. 6. It was discovered that at 620 K, the homogeneity region of γ-phase shifts partially to the cadmium chalcogenide-rich side, and a two-phase region (γ + α) appears at the section at this temperature. EDX analysis (Table 1) of the microsections of the two-phase alloys (the composition of the prevailing phase was determined) allows us to localize the position of one of the boundaries of the γ-phase. The next step was the preparation of several additional alloys (composition and location are shown in Fig. 1b) to determine the boundaries more accurately.

5.5. The '$CuCd_2InSe_4$'–'$CuCd_2InS_4$' section (Fig. 7)

The phase diagram of the '$CuCd_2InSe_4$'–'$CuCd_2InS_4$' section is shown in Fig. 7. The section liquidus consists of one line that corresponds to the beginning of the primary crystallization of β-solid solutions. Its homogeneity region decreases at lower temperature, occupying at 620 K somewhat more than half of the concentration range. The formation of a phase with a cubic structure occurs instead. The $\beta \Leftrightarrow \gamma$ transition is recorded by DTA only at high temperatures, therefore it is marked out on the diagram based on its position in the $CuInSe_2$–$2CdSe$ system and on X-ray phase analysis results.

5.6. The $CuInS_2$–$2CdSe$ section (Fig. 8)

The phase diagram of the $CuInS_2$–$2CdSe$ section that corresponds to one of the diagonals of the concentration quadrangle is presented in Fig. 8. The liquidus and the solidus of the section are represented by the lines of the

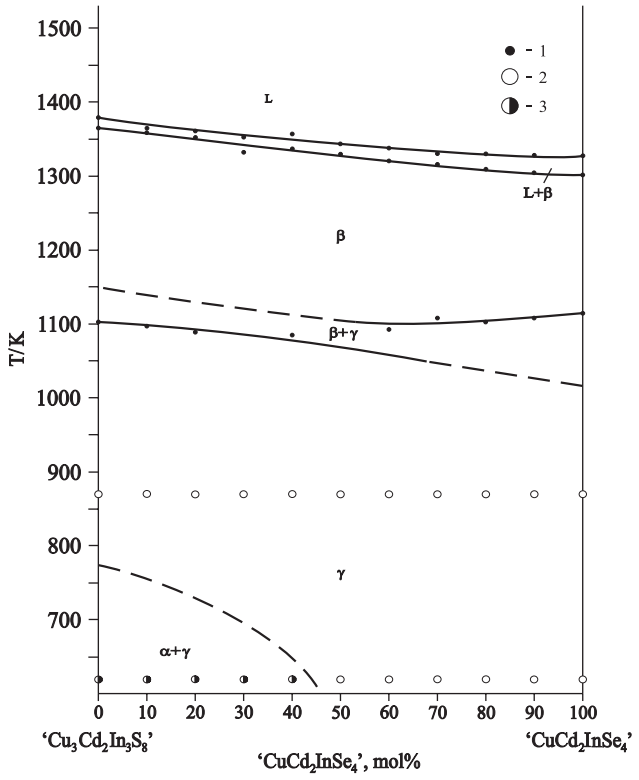

Fig. 5. Phase diagram of the '$Cu_3Cd_2In_3S_8$'–'$CuCd_2InSe_4$' section (1, DTA results; 2, single-phase alloys; 3, two-phase alloys).

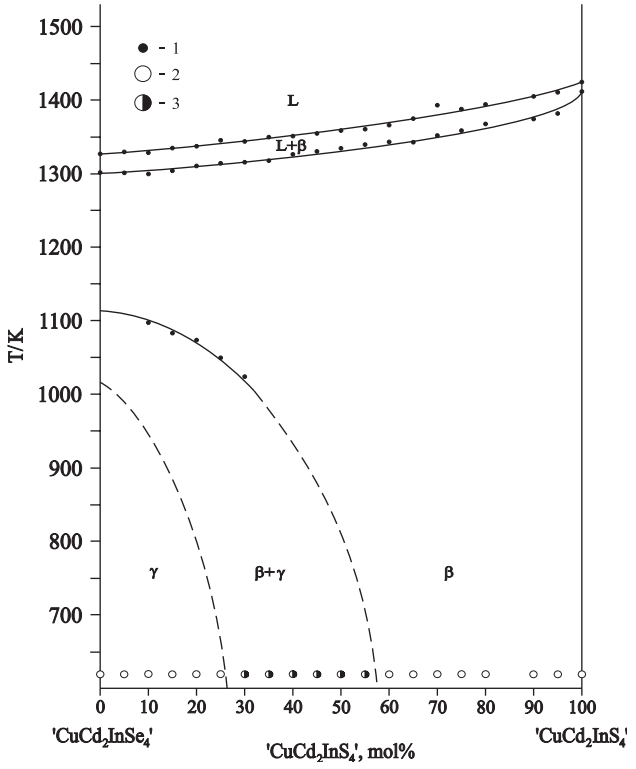

Fig. 7. Phase diagram of the '$CuCd_2InS_4$'–'$CuCd_2InSe_4$' section (1, DTA results; 2, single-phase alloys; 3, two-phase alloys).

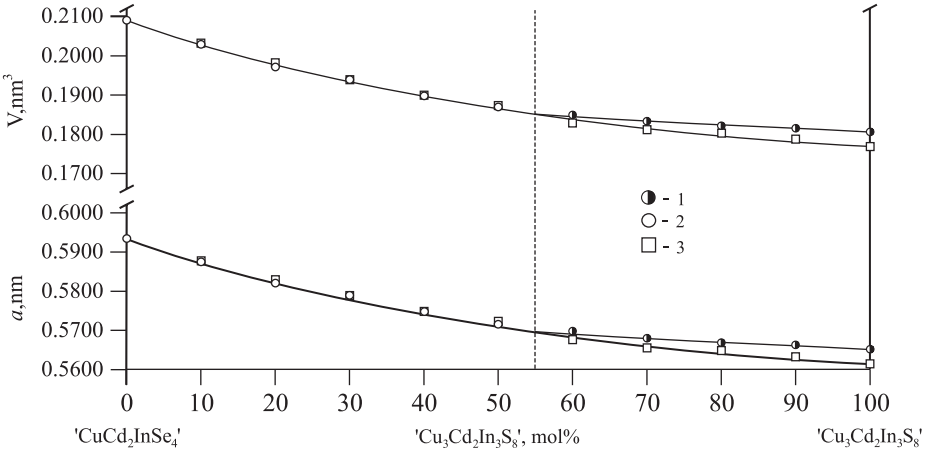

Fig. 6. Plots of the lattice parameters and unit cell volumes of the '$Cu_3Cd_2In_3S_8$'–'$CuCd_2InSe_4$' section alloys (1, two-phase alloys at 620 K; 2, single-phase alloys at 620 K; 3, single-phase alloys at 870 K).

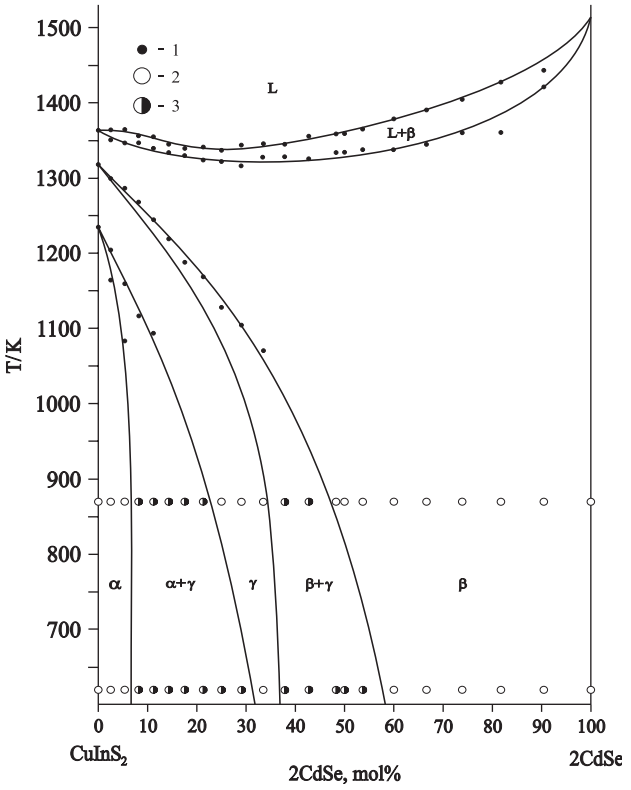

Fig. 8. Phase diagram of the $CuInS_2$–2CdSe section (1, DTA results; 2, single-phase alloys; 3, two-phase alloys).

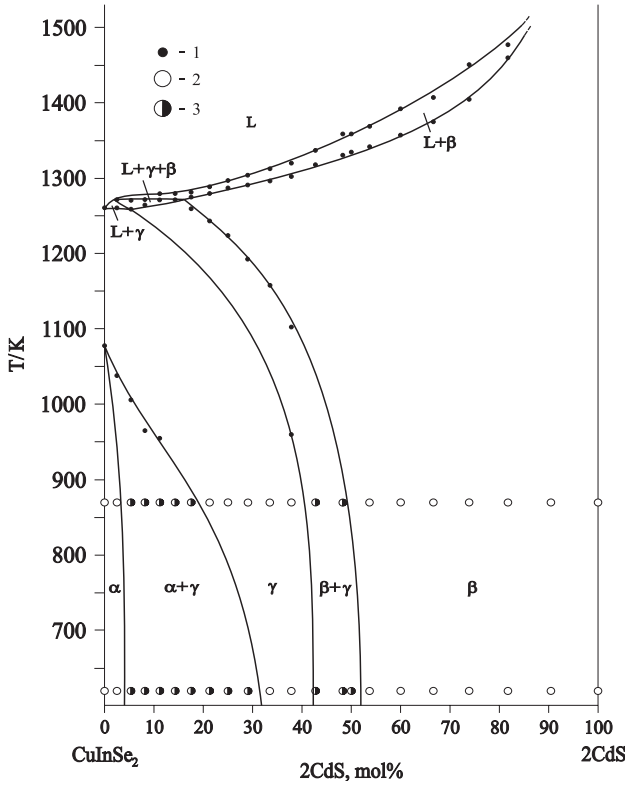

Fig. 9. Phase diagram of the $CuInSe_2$–2CdS section (1, DTA results; 2, single-phase alloys; 3, two-phase alloys).

beginning and the end of the primary crystallization of β-solid solutions; these are somewhat curved to the abscissa side. In sub-solidus part, a partial decomposition of β-solid solutions with the formation of γ-phase and, later, α-solid solutions takes place. The homogeneity regions of solid solutions were determined from the results of X-ray phase analysis of alloys annealed at different temperatures and of DTA. The XRD patterns of the alloys annealed at 620 K and 870 K contain one of three sets of diffraction reflections (that belong to the three known solid solutions) or their combination. The shift of the position of major peaks of the diffraction patterns is observed even in the two-phase region, which is reflected also in the change of the unit cell parameters of the alloys annealed at different temperatures. This means that different boundary α-, β- and γ-solid solutions are formed in different concentration ranges of the two-phase region. Therefore, the $CuInS_2$–2CdSe section is considered non-quasi-binary.

5.7. The $CuInSe_2$–2CdS section (Fig. 9)

The $CuInSe_2$–2CdS section coincides with the other quadrangle diagonal. Its phase diagram is given in Fig. 9, and is similar to the previous one. The difference is in the extent of the homogeneity regions of the phases and the appearance of another three-phase field in the sub-liquidus part that belongs to the region of the secondary crystallization of the only monovariant process that occurs in the system.

5.8. The '$Cu_2CdInSe_4$'–$CuInS_2$ and '$Cu_2CdInSe_4$'–CdS sections (Figs. 10 and 11)

The '$Cu_2CdInSe_4$'–$CuInS_2$ and '$Cu_2CdInSe_4$'–CdS sections were studied to establish the extent of solid solution ranges at 870 K. Both sections are described by the existence of two solid solution regions. In the former, they are solid solutions with the sphalerite and the chalcopyrite structure, in the latter, the sphalerite and the wurtzite structure. The change of the lattice parameters was observed in the two-phase region as well, therefore the solubility limits were determined by the microstructure analysis in addition to the XRD data.

5.9. The liquidus surface projection of the reciprocal system $CuInSe_2$+2CdS ⇔ $CuInS_2$+2CdSe (Fig. 12)

The liquidus surface projection of the reciprocal system $CuInSe_2 + 2CdS \Leftrightarrow CuInS_2 + 2CdSe$ (Fig. 12) was constructed based on the literature data on the CdS–CdSe [20], $CuInS_2$–CdS [25], $CuInSe_2$–CdSe [26] systems and on present results of the investigation of the above-mentioned sections. It consists of two fields of primary crystallization that correspond to β- and γ-solid solutions. The field of β-phase as the solid solution range of the phases with the

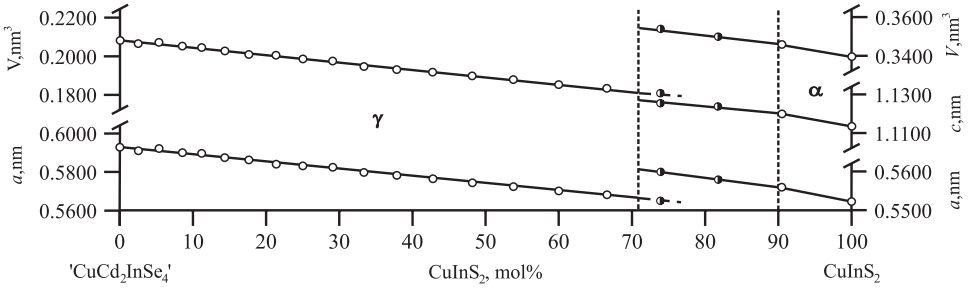

Fig. 10. Plots of the lattice parameters and unit cell volumes of the '$CuCd_2InSe_4$'–$CuInS_2$ section alloys.

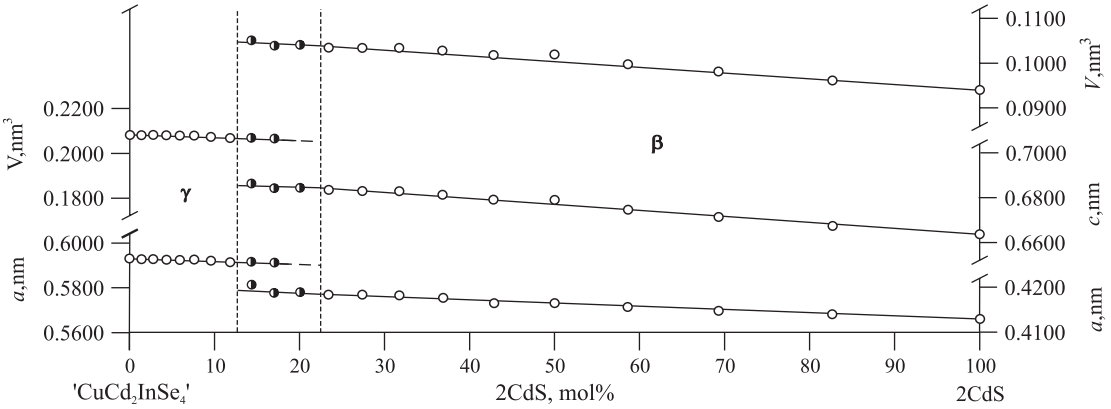

Fig. 11. Plots of the lattice parameters and unit cell volumes of the '$CuCd_2InSe_4$'–2CdS section alloys.

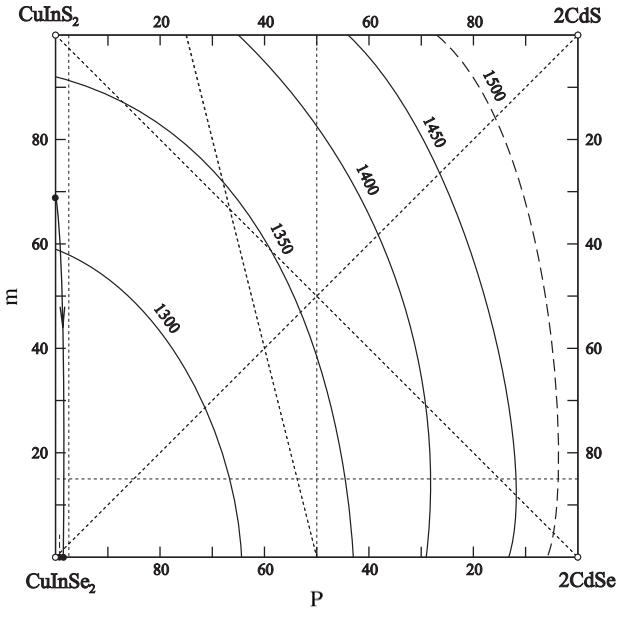

Fig. 12. Liquidus surface projection of the reciprocal system $CuInSe_2 + 2CdS \Leftrightarrow CuInS_2 + 2CdSe$.

highest melting points occupies the large part of the concentration quadrangle. The field of γ-solid solutions is minor and is localized near the quasi-binary system $CuInS_2$–$CuInSe_2$. The fields of primary crystallization are separated by a monovariant line *mp*. The isothermal lines of the liquidus are somewhat curved to the side of cadmium chalcogenides.

5.10. Perspective representation of the $CuInSe_2+2CdS \Leftrightarrow CuInS_2+2CdSe$ system (Fig. 13)

Due to the occurence of solid-state processes and significant solid solutions, it is advisable to consider a space version of the $CuInSe_2 + 2CdS \Leftrightarrow CuInS_2 + 2CdSe$ system (Fig. 13). Its base is a square, the edges are the compounds that form the system. Points *A*, *B*, *C* and *D* on the prism edges correspond to the melting point of the respective compounds. The prism faces are formed by the quasi-binary sections. The surface of the primary crystallization of β-solid solutions lies between points *BCDpmB*. The crystals of γ-solid solutions begin to crystallize on the surface *pAmp*. The secondary crystallization of the system is represented by one process related to the monovariant line that transforms as it goes on from a congruent ($\beta \Leftrightarrow \gamma + L$) to an incongruent one ($L + \beta \Leftrightarrow \gamma$). The volume of the secondary crystallization is limited by two horizontal lines ($m\gamma_2$ and $p\beta_3$) that lay on the bounding systems and by three lines in the middle of the reciprocal system (*mp*, $\beta_2\beta_3$ and $\gamma_2\gamma_1$). Based on the trasformation of the processes that take place in this volume, line $\beta_2\beta_3$ should be situated above line $\gamma_2\gamma_1$. The minimum in the liquidus line that

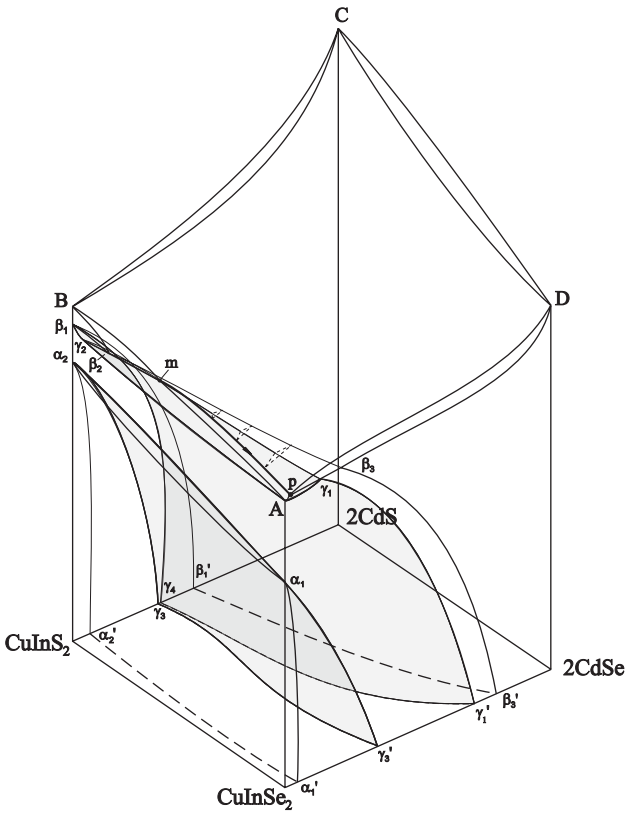

Fig. 13. Perspective view of the reciprocal system $CuInSe_2 + 2CdS \Leftrightarrow CuInS_2 + 2CdSe$.

occurs in the $CuInSe_2$–2CdSe system penetrates into the quadrangle and gradually levels off.

The $CuInSe_2 + 2CdS \Leftrightarrow CuInS_2 + 2CdSe$ system is of interest due to the formation of solid solutions. The field of γ-solid solution range of HT(1) modifications of ternary chalcogenides is limited by four surfaces. One of the surfaces ($\beta_1\gamma_2 A\alpha_1\alpha_2\beta_1$) is situated in the $CuInSe_2$–$CuInS_2$ system. Three other surfaces ($A\gamma_2\gamma_1 A$, $\beta_1\gamma_2\gamma_1\gamma_1'\gamma_4\beta_1$ and $\alpha_2\alpha_1\gamma_3'\gamma_3\alpha_2$) are shaded. The β-solid solution is located between surfaces $B\beta_2\beta_3 DCB$ and $\beta_1\beta_2\beta_3\beta_3'\beta_1'\beta_1$. Finally, α-solid solution is located in a narrow concentration range near the $CuInSe_2$–$CuInS_2$ system; within the reciprocal system it is limited by the $\alpha_2\alpha_1\alpha_1'\alpha_2'\alpha_2$ surface.

6. Conclusions

We have constructed the phase equlibria diagram of the reciprocal system $CuInSe_2 + 2CdS \Leftrightarrow CuInS_2 + 2CdSe$ which is characterized by the formation of extensive solid solutions. The existence of the solid solution with the cubic structure between $CuInSe_2$ and CdS may be the reason behind the change of the parameters of solar cells made of these compounds due to a solid-state process of its formation. The degradation analysis of the solar cells with the $CuInSe_2$/CdS heterojunction was performed by Meyer and van Dyk [27]. They established that the conversion coefficient of the module decreased by 26% over the period of $2\frac{1}{2}$ years. It was also established that a copper-rich nanolayer is formed at the heterojunction boundary; however, its chemical composition could not be determined accurately because its size is significantly smaller that the SEM electron beam diameter.

Physical properties of the intermediate alloys of the reciprocal system were not studied. However, considering the data on certain parameters of the alloys from the γ-phase region on the bounding sides (alloys of the $CuInS_2$–CdS section have *p*-type conductivity; γ-phase alloys on the $CuInSe_2$–CdSe section have bandgap energy 1.1–1.3 eV, *p*-type conductivity and are photosensitive), there are good starting conditions for an attempt to used the γ-phase alloys as a substitute material for $CuInSe_2$ in photovoltaic cells.

Acknowledgment

This work has been financially supported by the Science and Technology Centre in Ukraine (STCU), project Gr-91j.

References

[1] A. Goetzberger, C. Hebling, H.-W. Schock, Mater. Sci. Eng. R 40 (2003) 1.
[2] R.W. Miles, K.M. Hynes, I. Forbes, Prog. Cryst. Growth Charact. Mater. 51 (2005) 1.
[3] T. Surek, J. Cryst. Growth 275 (2005) 292.
[4] J. Tuttle, A. Szalaj, J. Keane, in: Proceedings of the 28th IEEE Photovoltaics Specialists Conference, Anchorage, 2000.
[5] V.Yu. Rud', Yu.V. Rud', Fiz. Tekh. Polyprovodnikov 33 (1999) 801.
[6] K. Ramanathan, M.A. Contreras, B. Egaas, F.S. Hasoon, R.N. Bhattacharya, R. Noufi, in: ICTMC-12, Proceedings of the 12th International Conference on Ternary Multinary Compounds, Taiwan, 2000.
[7] T. Coates, J. Mikin (Eds.), Current Problems of Semiconductor Photovoltaics, Mir, Moscow, 1988 (Russian translation).
[8] U. Rau, H.-W. Shock, Appl. Phys. A: Mater. Sci. Process. 69 (1999) 131.
[9] L. Kazmerski, Renew. Sustain. Energy Rev. 1 (1997) 71.
[10] V.F. Gremenok, I.V. Bodnar', V.Yu. Rud', Yu.V. Rud', H.-W. Schock, Fiz. Tekh. Poluprovodnikov 36 (2002) 360.
[11] R.W. Miles, K.T. Ramakrishna Reddy, I. Forbes, J. Cryst. Growth 198/199 (1999) 316.
[12] K.W. Mitchell, G.A. Pollock, A.V. Mason, in: Proceedings of the 20th IEEE Photovoltaics Specialists Conference, Las Vegas, 1988, p. 1542.
[13] T. Walter, A. Content, K.O. Velthaus, H.W. Schock, Sol. Energy Mater. Sol. Cell 26 (1992) 357.
[14] J. Djordjevic, C. Pietzker, R. Scheer, J. Phys. Chem. Sol. 64 (2003) 1843.
[15] M. Turchu, I.M. Kotschau, U. Rau, J. Appl. Phys. 91 (2002) 1391.
[16] M.A. Contreras, B. Egaas, K. Ramanathan, J. Hiltner, A. Swartzlander, F. Hasoon, R. Noufi, Prog. Photovolt. Res. Appl. 7 (1999) 311.
[17] V.B. Lazarev, Z.Z. Kish, E.Yu. Peresh, E.E. Semrad, Complex Chalcogenides in A^I–B^{III}–C^{VI} Systems, Metallurgiya, Moscow, 1993 (in Russian).
[18] S.G. Konnikov, G.A. Medvedkin, M.M. Sobolev, S.A. Solov'ev, Fiz. Tekh. Poluprovodnikov 31 (1997) 114.
[19] V.Y. Anosov, M.I. Ozerova, Y.Y. Fialkov, Essentials of Physical–Chemical Analysis, Nauka, Moscow, 1976 (in Russian).
[20] I.B. Mizetskaya, G.S. Oleinik, L.D. Budennaya, V.N. Tomashik, N.D. Oleinik, Physical-Chemical Basis of the Single Crystal Synthesis

of Semiconductor $A^{II}B^{VI}$-based Solid Solutions, Naukova Dumka, Kyiv, 1986 (in Russian).
[21] V.N. Tomashik, V.I. Grytsiv, Phase diagrams based on semiconductor compounds $A^{II}B^{VI}$. Naukova Dumka, Kyiv, 1982, in Russian.
[22] I.D. Olekseyuk, O.A. Husak, L.D. Gulay, O.V. Parasyuk, J. Alloy Compd. 367 (2004) 25.
[23] B. Krebs, D. Voelker, K.-O. Stiller, Anorg. Chim. Acta 68 (1982) L101.
[24] E.N. Kholina, V.B. Ufimtsev, A.S. Timoshin, Neorg. Mater. 15 (1979) 1918.
[25] I.D. Olekseyuk, G.Ye. Davidyuk, O.V. Parasyuk, S.V. Voronyuk, V.O. Halka, V.A. Oksyuta, J. Alloy Compd. 309 (2000) 39.
[26] I.D. Olekseyuk, O.V. Parasyuk, O.A. Husak, L.V. Piskach, J. Sol. State Chem. 179 (2006) 315.
[27] E.L. Meyer, E.E. van Dyk, Phys. Stat. Sol. (a) 201 (2004) 2245.